Supporting Information:

Investigations of Metal Phosphides as Potential Thermoelectric Materials

Jan-Hendrik Pöhls,[a] Alireza Faghaninia,[b] Guido Petretto,[c] Umut Aydemir,[d, e] Francesco Ricci,[c] Guodong Li,[f] Max Wood,[d] Saneyuki Ohno,[d,g] Geoffroy Hautier,[c] G. Jeffrey Snyder,[d] Gian-Marco Rignanese,[c] Anubhav Jain,[b] and Mary Anne White [a,h,i]

[a] Department of Physics and Atmospheric Science, Dalhousie University, 6310 Coburg Rd, PO BOX 15000, Halifax, NS, B3H 4R2 Canada

[b] Lawrence Berkeley National Lab, 1 Cyclotron Rd, Berkeley, CA, USA

[c] Institute of Condensed Matter and Nanosciences (IMCN), Université catholique de Louvain, Chemin des Étoiles 8, B-1348 Louvain-la-Neuve, Belgium

[d] Department of Materials Science and Engineering, Northwestern University, 2220 Campus Drive, Evanston, IL-60208, USA

[e] Department of Chemistry, Koc University, Sariyer, Istanbul 34450, Turkey

[f] State Key Laboratory of Advanced Technology for Materials Synthesis and Processing, Wuhan University of Technology, Wuhan 430070, China

[g] Department of Applied Physics and Materials Science, California Institute of Technology, 1200 E. California Blvd. Pasadena, CA 91125, USA

[h] Clean Technologies Research Institute, Dalhousie University, Halifax, NS B3H 4R2, Canada

[i] Department of Chemistry, Dalhousie University, Halifax, NS B3H 4R2, Canada

*Author for correspondence; email: mawhite@dal.ca; Tel: 902-494-3894; website: http://mawhite.chem.dal.ca/

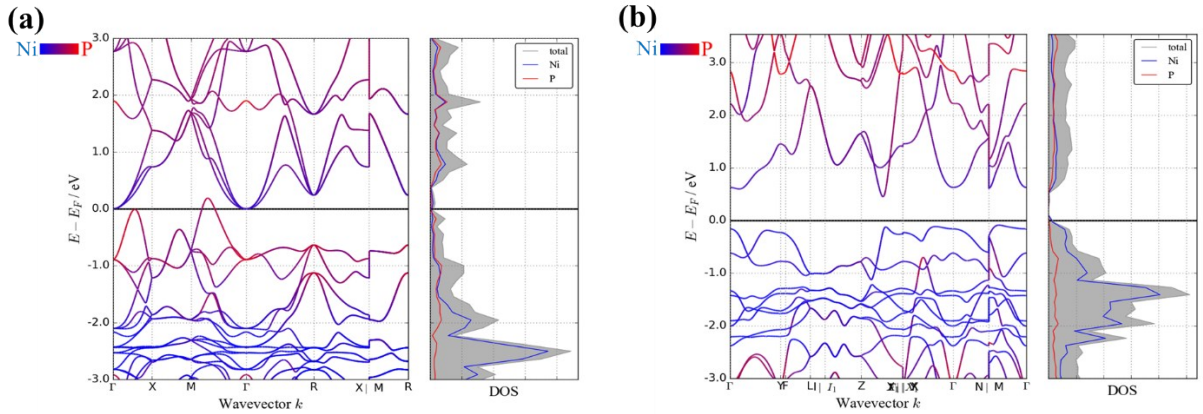

Figure S1: Electronic band structure of (a) cubic NiP_2 (mp-22619) and (b) monoclinic NiP_2 (mp-486) computed with DFT-PBE-GGA.

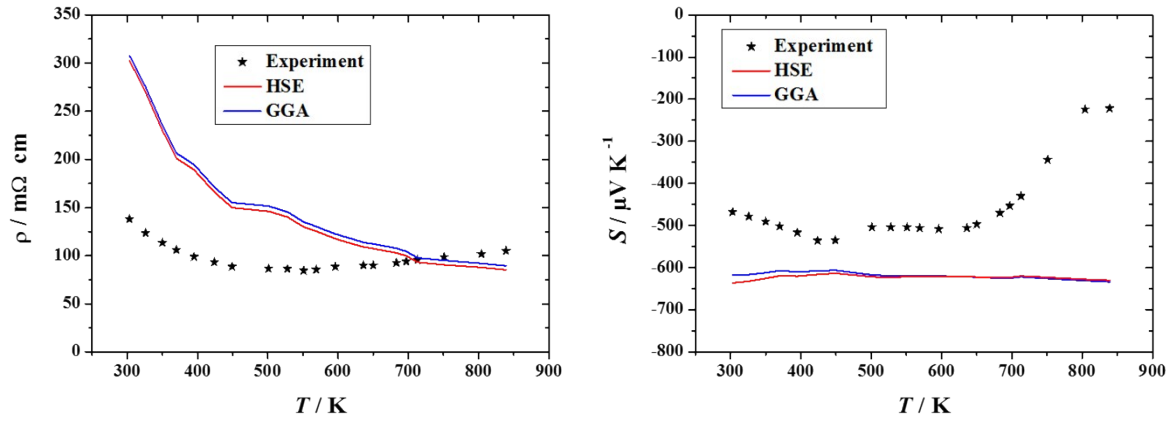

Figure S2: Comparison between computed electrical resistivity and Seebeck coefficient of BP to experimental values reported by Kumashiro *et al.*[1] While the computed resistivity is similar to experiments, the magnitude of the computed Seebeck coefficient is overestimated.

1. Minimum thermal conductivity models

The most established model to determine the amorphous limit is the Cahill-Pohl model [2,3] with

$$\kappa_{min,CP} = \frac{1}{2.48} k_B \left(\frac{N}{V}\right)^{2/3} (v_L + 2v_T) \qquad \text{SI-1}$$

where k_B is the Boltzmann constant, N is the total number of atoms in the unit cell volume V, and v_L and v_T are the longitudinal and transverse speeds of sound, respectively. The speeds of sound were calculated from the computed elastic constants using first-principle calculations and a Voigt-Reuss-Hill average; the stress-strain method used for these calculations is described elsewhere.[4] The longitudinal and transverse speeds of sound, therefore, are given by

$$v_L = \left(\frac{K + 4/3G}{d}\right)^{1/2} \quad \text{SI-2}$$

and

$$v_T = \left(\frac{G}{d}\right)^{1/2}, \quad \text{SI-3}$$

where K is the bulk modulus and G is the shear modulus.

In a recent report, we demonstrated that the experimental phononic contribution of the thermal conductivity has a strong correlation with the amorphous thermal conductivity.[5] However, several materials showed thermal conductivity lower than the predicted amorphous limit; the thermal conductivity in these materials is defined as 'ultralow'. In a recent study, the origins of the ultralow thermal conductivity of [6,6]-phenyl-C_{61}-butyric acid methyl ester (PCBM) was delineated.[6] As shown in Equation SI-1 the amorphous limit is calculated from the speed of sound which is taken from the linear slope of the acoustic phonons near the center of the Brillouin zone. However, a small phonon mean free path (λ) has a large wavevector ($k = \frac{2\pi}{\lambda}$) and using the linear slope at the center of the Brillouin zone overestimates the phonon mean speed, $\bar{v}$. Therefore, the mean phonon speed over the entire Brillouin zone was calculated for the longitudinal and transverse acoustic phonons. The three phonon mean speeds were averaged by

$$\langle \bar{v} \rangle = \left(\frac{1}{3}\left[\frac{1}{\bar{v}_L^3} + \frac{1}{\bar{v}_{T1}^3} + \frac{1}{\bar{v}_{T2}^3}\right]\right)^{-1/3} \quad \text{SI-4}$$

and an average Debye temperature, $\langle \theta_D \rangle$, was computed from

$$\langle \theta_D \rangle = \frac{\langle \bar{v} \rangle \hbar}{k_B}\left(\frac{6\pi^2 N}{V}\right) \quad \text{SI-5}$$

where $\hbar$ is the reduced Planck constant. The thermal conductivity in a material can be limited by a constant phonon mean free path $\left(\lambda = \left[\frac{\pi V}{6N}\right]^{1/3}\right)$ [6] and a frequency-dependent phonon mean free path $\left(\lambda = \frac{\pi}{\omega}\langle \bar{v} \rangle\right)$ as assumed by Einstein.[7] While the latter does not allow for the grain boundary limit for low frequencies, it can represent the limit where dynamical disorder is responsible for the low thermal conductivity (referred as 'dynamic'). The constant mean free path, on the other hand, can delineate the limit for static disordering (referred as 'static') which was most likely the

case for the ultralow thermal conductivity in PCBM and C_{60}/C_{70}.[6] The thermal conductivities for the static and dynamic disordering are calculated by $\langle\theta_D\rangle$ (Equation SI-5) and the atomic density (N/V)

$$\kappa_{min,st}(T) = \frac{3}{6^{2/3}\pi^{1/3}}\frac{k_B^2}{\hbar}\left(\frac{N}{V}\right)^{1/3}\frac{\langle\theta_D\rangle}{x_D^3}\int_0^{x_D}\frac{x^4e^x}{(e^x-1)^2}dx \qquad \text{SI-6}$$

and

$$\kappa_{min,dy}(T) = \frac{3}{6^{2/3}\pi^{1/3}}\frac{k_B^2}{\hbar}\left(\frac{N}{V}\right)^{1/3}\frac{\langle\theta_D\rangle}{x_D^2}\int_0^{x_D}\frac{x^3e^x}{(e^x-1)^2}dx \qquad \text{SI-7}$$

respectively, where $x_D = \frac{\langle\theta_D\rangle}{T}$. More information of the derivation of these models can be found in reference [6].

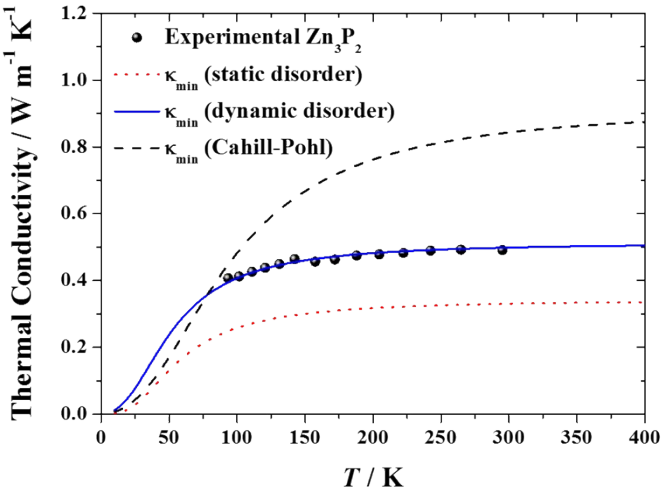

Figure S3: Ultralow thermal conductivity in Zn_3P_2[**Error! Bookmark not defined.**] can be explained using an average phonon mean speed from phonon band calculations. While static disordering (frequency-independent phonon mean free path) predicts a lower thermal conductivity, dynamic disordering (frequency-dependent mean free path) agrees well with the experiments.

2. Characterization of *c*-NiP_2

While the monoclinic phase of NiP_2 indicates better predicted TE performance than the cubic phase, the synthesis of the former using a solid-state approach as reported by Gillot *et al.*[8] was not successful and toxic phosphine gas was produced. Using high-energy ball milling, pure *c*-NiP_2 was synthesized. The crystal structure of *c*-NiP_2 is pyritic where Ni and P occupy octahedral and tetrahedral environments, respectively (Figure S4). The crystal structure of *c*-NiP_2 was confirmed by powder X-ray diffraction (PXRD) analysis (Figure S5 (a)). The refined lattice parameter of the cubic structure (a = 5.469(2) Å) is close to the reported value of 5.4706(2) Å[9] and to that in our computed structure (5.453 Å). In the crystal structure, each P is bonded to one P and three Ni, while each Ni is surrounded by six P atoms (Figure S4 (a)). The tetrahedral (for P) and octahedral (for Ni) environments are slightly distorted. Electron localization function (ELF) calculations show shared electrons for Ni-P indicating polar covalent bonding (Figure S4 (b)). A Bader charge analysis demonstrated that the charge transfer between Ni (+0.11) and P (-0.04; -0.07) is subtle, due to the similar electronegativity of Ni (1.91) and P (2.19). The PXRD spectrum showed broad peaks indicating small grains (Figure S5 (a)). From the Rietveld refinement it was found that the reflections can be fitted only with Lorentzian functions and therefore, the grain size can be determined using a Hall-Williamson plot.[10] With the Hall-Williamson plot the peak broadening due to the grain size as well as inhomogeneous strain can be determined (see inset of Figure S5 (a)). From the intercept of the linear fit a grain size of 19±1 nm was determined. This is consistent with the SEM image, which indicates grains in the range of 10 to 20 nm (see Figure S5 (b)). In addition to the grain size, SEM reveals that the *c*-NiP_2 sample contains pores in the range of 10 to 30 nm which results in a reduced density (4.04 g cm^{-3}) compared to the computed theoretical density (4.94 g cm^{-3}). The charge transfers of the other MPs are summarized in Table S9.

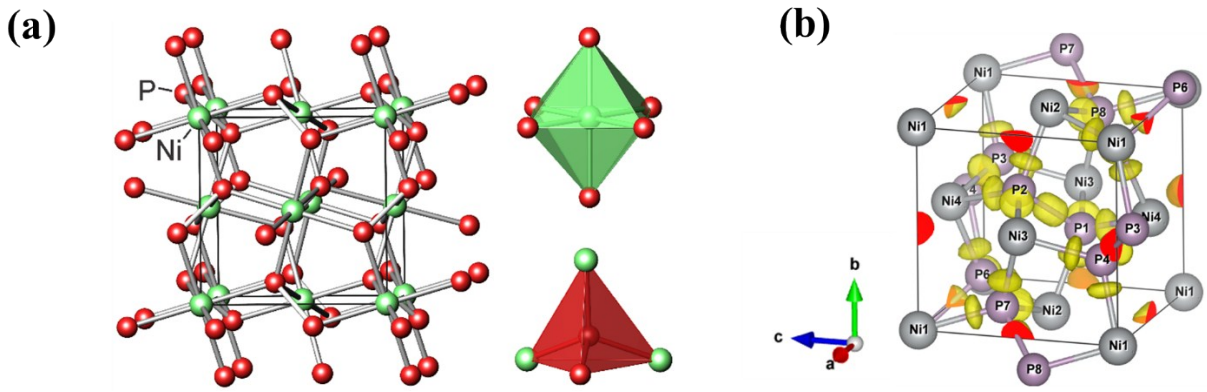

Figure S4: (a) Crystal structure and (b) electron localization function (ELF) calculation of cubic NiP_2. Each P atom is tetrahedrally bonded to three Ni atoms (P $^{-0.07;-0.04}$; Ni $^{+0.11}$) and one P atom; each Ni atom fills the octahedral interstices. The electron densities are found closer to the P atom for Ni-P and at the bond middle point for P-P indicating polar covalent and pure covalent interactions, respectively.

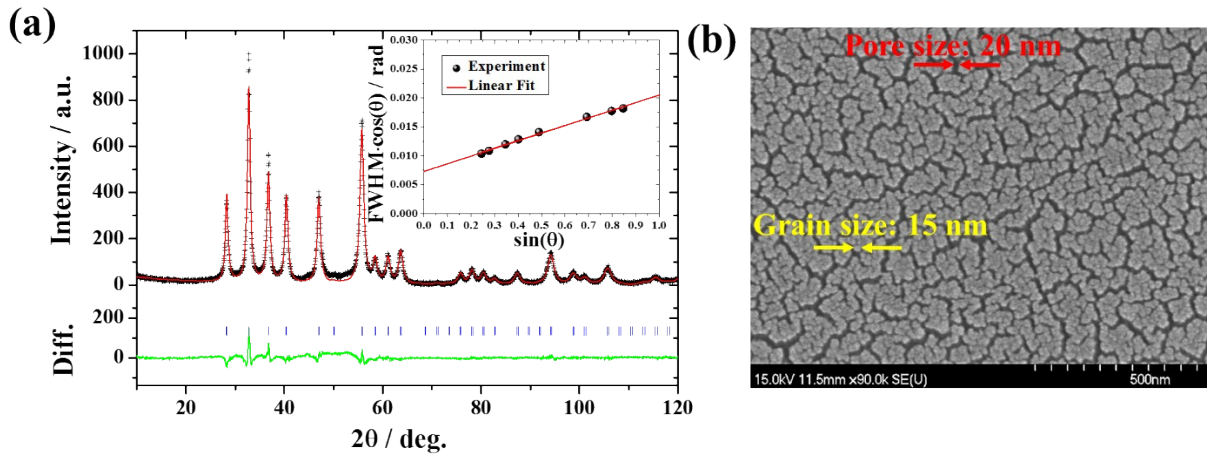

Figure S5: (a) Rietveld refinement pattern of cubic NiP_2 (space group: $Pa\bar{3}$). Blue tick marks show the calculated reflections and the green baseline corresponds to the residuals of the Rietveld refinement. Inset: Hall-Williamson plot gives a grain size of 19±1 nm. (b) SEM image of the surface of a consolidated NiP_2 pellet, showing grains in the range of 10 to 20 nm.

The temperature stability of *c*-NiP_2 is shown in Figure S6 (a). A mass increase was observed at approximately 470 °C, following a decrease in mass from 570 °C to 730 °C. Although the measurement was conducted under inert atmosphere, the increase in mass can be assigned to oxidation of NiP_2 to $Ni(PO_3)_2$ as observed by the minor phase in PXRD after the thermogravimetric measurement (Figure S6 (b)). At higher temperatures (T > 570 °C), P is removed from the non-oxidized NiP_2 until it is completely converted to $Ni_{12}P_5$.

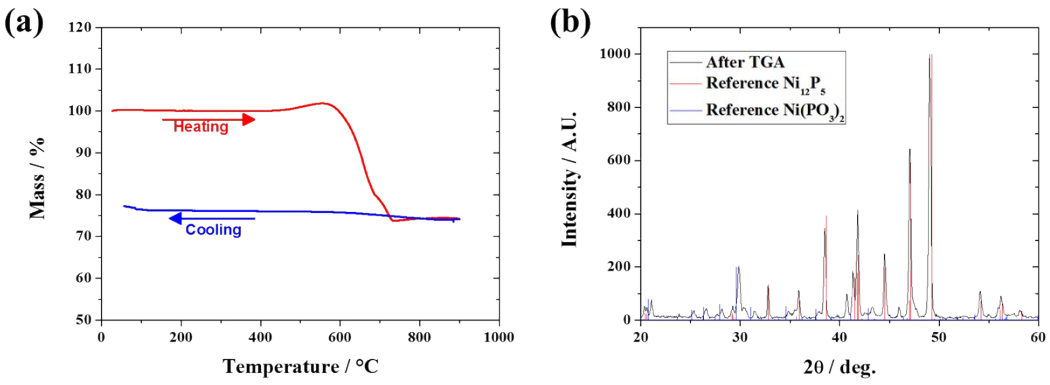

Figure S6: (a) Thermogravimetric analysis of NiP_2 indicates major decomposition sets in at 570 °C. (b) PXRD pattern of sample after TGA shows the major phase is $Ni_{12}P_5$ with a minor phase of $Ni(PO_3)_2$.

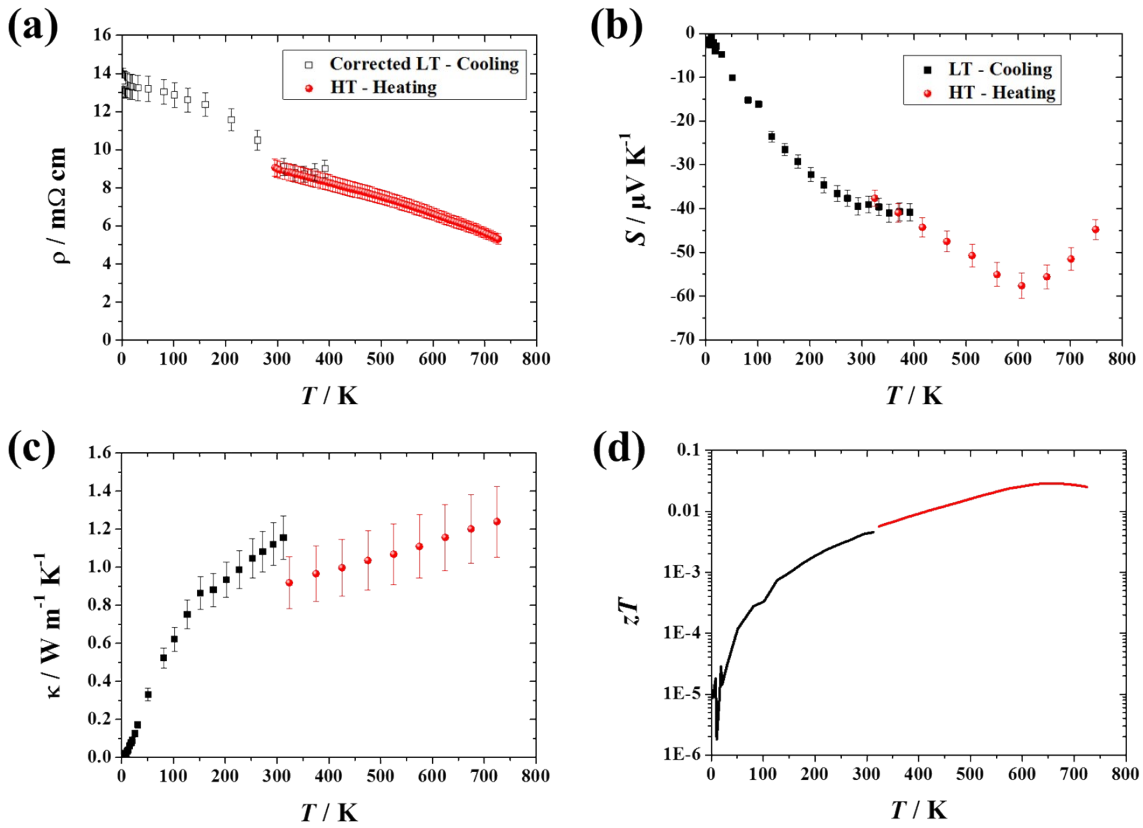

Figure S7. The experimental (a) electrical resistivity, ρ, (b) Seebeck coefficient, *S*, (c) thermal conductivity, κ, and (d) figure of merit of *c*-NiP_2 as functions of temperature, *zT*.

Table S1: Computed electronic transport properties for different *p*-type metal phosphorous compounds at $n = 10^{20}$ cm^{-3} and the temperature where the predicted zT_{calc} is maximum. The electronic transport properties were calculated from the PBE band structures with the Boltztrap code where the constant relaxation time was set to 10^{-14} s.

Material	mp-id	Space group	E_g / eV HSE (PBE)	T / K	S / μV K^{-1}	ρ / mΩ cm	κ_{el} / W m^{-1} K^{-1}	PF / mW m^{-1} K^{-2}
BP	1479	216	1.98 (1.24)	1300	318	1.39	1.67	7.28
GaP	2490	216	(1.59)	1300	339	1.67	1.43	6.88
InP	20351	216	(0.47)	1100	324	1.89	1.26	5.54
FeP	1005	62	0.00 (0.00)	1300	39	0.09	38.73	1.69
ZnNaP	4824	129	(0.91)	1300	356	2.26	1.43	5.61
SrLiP	10614	187	(0.80)	1000	378	3.13	0.87	4.56
BaLiP	10615	187	(0.70)	1100	341	2.96	0.03	3.93
SnNaP	29529	186	(0.58)	800	291	1.92	0.10	4.41
NiP_2	22619	205	0.13 (0.00)	700	80	0.17	16.35	3.76
NiP_2	486	15	1.15 (0.53)	500	357	2.55	0.00	5.00
ZnP_2	11025	96	2.20 (1.46)	1300	366	7.93	0.17	1.69
ZnP_2	2782	92	2.20 (1.46)	1300	365	7.93	0.17	1.68
AgP_2	8200	14	1.30 (0.66)	1100	278	2.27	0.99	3.40
TiP_2	20327	62	0.00 (0.00)	1100	31	0.1	37.01	0.96
CuP_2	927	14	(0.86)	1100	350	2.81	0.74	4.36
RuP_2	1413	58	(0.48)	800	307	2.08	0.98	4.53
CoP_2	14285	14	(0.44)	700	290	2.72	0.53	3.09
IrP_2	10155	14	(0.78)	1100	329	2.07	1.04	5.23
BeP_2	27148	15	(0.83)	1300	315	2.13	1.55	4.66
RhP_2	15953	14	(0.37)	800	265	1.62	1.30	4.33
PdP_2	28266	15	(0.46)	600	298	2.3	0.58	3.86
FeP_2	20027	58	(0.43)	500	442	12.8	0.09	1.53
Zn_3P_2	2071	137	1.17 (0.31)	900	278	1.76	1.04	4.39
Mg_3P_2	8085	224	(1.11)	1200	451	6.56	0.24	3.10
Mg_3P_2	2514	206	2.20 (1.61)	1300	408	8.4	0.16	1.98
Cd_3P_2	2441	137	0.65 (0.002)	600	224	1.97	0.86	2.55
MnP_4	569522	2	(0.48)	700	315	9.83	0.26	1.01
MnP_4	487	2	1.58 (0.44)	700	343	5.78	0.38	2.04
PbTe	19717	225	(0.81)	1100	419	1.08	1.97	16.26
Bi_2Te_3	568390	166	(0.25)	1000	315	1.46	2.02	6.80

Table S2: Computed electronic transport properties for different *n*-type metal phosphorous compounds at $n = 10^{20}$ cm^{-3} and the temperature where the predicted zT_{calc} is maximum. The electronic transport properties were calculated from the PBE band structures with the Boltztrap code where the constant relaxation time was set to 10^{-14} s.

Material	mp-id	Space group	E_g / eV HSE (PBE)	T / K	S / μV K^{-1}	ρ / mΩ cm	κ_{el} / W m^{-1} K^{-1}	PF / mW m^{-1} K^{-2}
BP	1479	216	1.98 (1.24)	1300	-339	1.46	1.79	7.87
GaP	2490	216	(1.59)	1300	-368	1.14	2.22	11.88
InP	20351	216	(0.47)	1300	-113	0.73	6.67	1.76
FeP	1005	62	0.00 (0.00)	1300	-39	0.09	38.77	1.69
ZnNaP	4824	129	(0.91)	1300	-288	1.29	0.86	6.43
SrLiP	10614	187	(0.8)	1000	-345	4.04	0.61	2.95
BaLiP	10615	187	(0.7)	1100	-338	2.6	0.42	4.39
SnNaP	29529	186	(0.58)	900	-257	1.24	1.36	5.33
NiP_2	22619	205	0.13 (0.00)	800	-69	0.17	21.50	2.8
NiP_2	486	15	1.15 (0.53)	800	-242	1.03	1.76	5.69
ZnP_2	11025	96	2.20 (1.46)	1300	-333	5.56	0.73	1.99
ZnP_2	2782	92	2.20 (1.46)	1300	-333	5.57	0.73	1.99
AgP_2	8200	14	1.30 (0.66)	1000	-325	2.56	0.81	4.13
TiP_2	20327	62	0.00 (0.00)	1100	-34	0.1	37.03	1.16
CuP_2	927	14	(0.86)	1100	-350	3.29	0.98	3.72
RuP_2	1413	58	(0.48)	800	-274	2.86	0.70	2.63
CoP_2	14285	14	(0.44)	600	-390	4.4	0.27	3.46
IrP_2	10155	14	(0.78)	1000	-264	4.28	0.68	1.63
BeP_2	27148	15	(0.83)	1300	-334	2.46	1.52	4.53
RhP_2	15953	14	(0.37)	600	-322	6.58	0.32	1.58
PdP_2	28266	15	(0.46)	700	-248	1.15	1.02	5.35
FeP_2	20027	58	(0.43)	700	-293	4.73	0.67	1.81
Zn_3P_2	2071	137	1.17 (0.31)	1100	-201	1.39	3.03	2.91
Mg_3P_2	8085	224	(1.11)	1300	-295	1.61	1.93	5.41
Mg_3P_2	2514	206	2.20 (1.61)	1300	-242	1.51	1.70	3.88
Cd_3P_2	2441	137	0.65 (0.002)	1200	-142	0.77	5.72	2.62
MnP_4	569522	2	(0.48)	700	-351	14.66	0.12	0.84
MnP_4	487	2	1.58 (0.44)	700	-362	4.43	0.39	2.96
PbTe	19717	225	(0.81)	1300	-343	0.95	5.35	12.38
Bi_2Te_3	568390	166	(0.25)	1100	-283	1.04	3.07	7.7

Table S3: Calculated power factors in *x*, *y*, and *z*-direction in the units mW m^{-1} K^{-2} at $n = 10^{20}$ cm^{-3} and $T = 600$ K. Note that a constant relaxation time of 10^{-14} s was used for the electronic transport property calculations.

Material	NiP_2	CoP_2	MnP_4	PdP_2	FeP_2	TiP_2	RuP_2	SrLiP	SnNaP	ZnNaP	BaLiP
mp-id	486	14258	487	28266	20027	20327	1413	10614	29529	4824	10615
n-PF_{xx}	1.36	1.54	2.47	2.71	0.96	0.25	2.04	1.66	2.72	2.28	1.37
n-PF_{yy}	6.67	3.48	4.05	3.99	1.88	2.04	2.83	1.66	4.18	2.28	1.37
n-PF_{zz}	2.48	5.35	2.28	6.06	2.55	0.95	1.15	3.28	4.18	0.33	2.21
p-PF_{xx}	1.37	2.01	1.85	2.73	1.33	0.45	3.05	2.38	0.84	6.39	1.57
p-PF_{yy}	5.73	2.89	1.93	4.87	0.95	1.80	3.51	2.38	0.84	6.39	1.57
p-PF_{zz}	5.08	2.97	1.79	3.25	1.97	0.89	4.86	6.90	7.70	0.36	3.14

Table S4: Computed *p*-type (*p*-PF) and *n*-type (*n*-PF) power factors of metal phosphorous compounds at 600 K and 10^{20} cm^{-3}. The electronic transport properties were calculated from the HSE and PBE-GGA band structures, respectively, with the Boltztrap code where the constant relaxation time was set to 10^{-14} s.

Material	mp-id	Space group	*p-PF* / mW m^{-1} K^{-2} (HSE)	*n-PF* / mW m^{-1} K^{-2} (HSE)	*p-PF* / mW m^{-1} K^{-2} (PBE-GGA)	*n-PF* / mW m^{-1} K^{-2} (PBE-GGA)
BP	1479	216	3.48	4.32	4.07	4.19
FeP	1005	62	0.0588	0.0517	0.838	0.847
NiP_2	22619	205	4.41	0.674	3.21	2.01
NiP_2	486	15	2.60	2.77	5.41	3.37
ZnP_2	11025	96	2.52	1.22	2.08	0.922
ZnP_2	2782	92	2.52	1.22	2.08	0.921
AgP_2	8200	14	1.66	1.79	2.19	2.92
TiP_2	20327	62	0.366	0.362	1.05	1.06
Zn_3P_2	2071	137	1.86	1.40	3.59	1.14
Mg_3P_2	2514	206	1.56	1.66	2.09	1.44
Cd_3P_2	2441	137	2.05	0.36	2.54	0.70
MnP_4	487	2	2.25	2.60	2.09	1.44

***Table S5*:** Minimum thermal conductivity using different models. Using static disordering and an average phonon mean speed indicates the amorphous limit. The minimum thermal conductivities using the Cahill-Pohl model where the speed of sounds were calculated from bulk and shear moduli predict the highest values and were taken to calculate the theoretical zT_{calc} in Figure 5.

	Material	κ_{min} (Cahill-Pohl, bulk)	κ_{min} (Cahill-Pohl, phonon)	κ_{min} (static disorder, avg. phonon)	κ_{min} (dynamic disorder, avg. phonon)
mp-22619	NiP_2	1.6	1.36	0.81	1.22
mp-486	NiP_2	1.32	1.06	0.53	0.8
mp-1479	BP	2.81	2.43	0.89	1.34
mp-2490	GaP	0.97	0.68	0.27	0.4
mp-8200	AgP_2	0.95	0.58	0.39	0.58
mp-2071	Zn_3P_2	0.92	0.71	0.34	0.51
mp-2782	ZnP_2	1.14	0.86	0.39	0.58
mp-11025	ZnP_2	0.97	0.86	0.47	0.71
mg-2514	Mg_3P_2	1.07	0.92	0.44	0.67
mp-487	MnP_4	1.77	1.57	0.91	1.41

Table S6: Comparison of computed thermal conductivity using the amorphous limit by Cahill and Pohl (κ_{min})[2,3] and using a semi-empirical approach described by Miller *et al.* (κ_{SE}) at 300 K.[11] All studied *XY*Ps have a low estimated thermal conductivity (< 2.5 W m^{-1} K^{-1}) using both approaches pointing to excellent high-performance TE materials.

Material	mp-id	Space group	κ_{min} / W m^{-1} K^{-1}	κ_{SE} / W m^{-1} K^{-1}
BP	1479	216	2.81	243.50
GaP	2490	216	0.97	47.74
InP	20351	216	0.62	27.10
FeP	1005	62	1.73	4.85
ZnNaP	4824	129	0.80	1.84
SrLiP	10614	187	0.79	2.12
BaLiP	10615	187	0.60	1.55
SnNaP	29529	186	0.52	1.75
c-NiP_2	22619	205	1.60	12.73
m-NiP_2	486	15	1.32	14.26
ZnP_2	11025	96	0.97	6.36
ZnP_2	2782	92	1.14	6.36
AgP_2	8200	14	0.95	4.18
TiP_2	20327	62	1.60	4.88
CuP_2	927	14	1.12	6.90
RuP_2	1413	58	1.66	13.2
CoP_2	14285	14	1.78	9.69
IrP_2	10155	14	1.24	10.15
BeP_2	27148	15	9.19	10.90
RhP_2	15953	14	1.51	9.65
PdP_2	28266	15	1.03	13.12
FeP_2	20027	58	2.00	13.36
Zn_3P_2	2071	137	0.92	2.60
Mg_3P_2	8085	224	1.14	4.18
Mg_3P_2	2514	206	1.07	4.21
Cd_3P_2	2441	137	0.52	1.84
MnP_4	569522	2	1.78	8.44
MnP_4	487	2	1.77	20.65
PbTe	19717	225	0.35	2.26
Bi_2Te_3	568390	166	0.22	0.56

Table S7: zT_{calc} for different *p*-type metal phosphorous compounds at $n = 10^{20}$ cm^{-3} and the temperature where the predicted zT_{calc} (κ_{min}) is maximum. The thermal conductivity is calculated using the amorphous limit by Cahill and Pohl (κ_{min})[2,3] and a semi-empirical approach by Miller *et al* (κ_{SE}).[10] The electronic transport properties were calculated from the PBE band structures with the Boltztrap code where the constant relaxation time was set to 10^{-14} s.

Material	mp-id	Space group	T / K	zT_{calc} (κ_{min})	zT_{calc} (κ_{SE})
BP	1479	216	1300	2.11	0.16
GaP	2490	216	1300	3.74	0.68
InP	20351	216	1100	3.24	0.66
FeP	1005	62	1300	0.06	0.05
ZnNaP	4824	129	1300	3.27	2.40
SrLiP	10614	187	1000	2.75	2.05
BaLiP	10615	187	1100	6.88	3.87
SnNaP	29529	186	800	5.69	2.42
NiP_2	22619	205	700	0.15	0.12
NiP_2	486	15	500	1.89	0.33
ZnP_2	11025	96	1300	1.94	0.62
ZnP_2	2782	92	1300	1.67	0.62
AgP_2	8200	14	1100	1.93	1.04
TiP_2	20327	62	1100	0.03	0.03
CuP_2	927	14	1100	2.59	1.10
RuP_2	1413	58	800	1.38	0.55
CoP_2	14285	14	700	0.93	0.38
IrP_2	10155	14	1100	2.52	1.07
BeP_2	27148	15	1300	0.56	0.90
RhP_2	15953	14	800	1.23	0.56
PdP_2	28266	15	600	1.43	0.29
FeP_2	20027	58	500	0.36	0.10
Zn_3P_2	2071	137	900	2.01	1.15
Mg_3P_2	8085	224	1200	2.69	1.19
Mg_3P_2	2514	206	1300	2.10	0.75
Cd_3P_2	2441	137	600	1.10	0.60
MnP_4	569522	2	700	0.35	0.12
MnP_4	487	2	700	0.66	0.14

PbTe	19717	225	1100	7.78	6.19
Bi_2Te_3	568390	166	1000	3.01	2.69

Table S8: zT_{calc} for different *n*-type metal phosphorous compounds at $n = 10^{20}$ cm^{-3} and the temperature where the predicted zT_{calc} (κ_{min}) is maximum. The thermal conductivity is calculated using the amorphous limit by Cahill and Pohl (κ_{min})[2,3] and a semi-empirical approach by Miller *et al* (κ_{SE}).[10] The electronic transport properties were calculated from the PBE band structures with the Boltztrap code where the constant relaxation time was set to 10^{-14} s.

Material	mp-id	Space group	T / K	zT_{calc} (κ_{min})	zT_{calc} (κ_{SE})
BP	1479	216	1300	2.23	0.17
GaP	2490	216	1300	4.84	0.92
InP	20351	216	1300	0.31	0.17
FeP	1005	62	1300	0.06	0.05
ZnNaP	4824	129	1300	5.06	3.39
SrLiP	10614	187	1000	2.11	1.45
BaLiP	10615	187	1100	4.71	3.27
SnNaP	29529	186	800	2.55	1.85
NiP_2	22619	205	700	0.10	0.08
NiP_2	486	15	500	1.49	0.59
ZnP_2	11025	96	1300	1.52	0.63
ZnP_2	2782	92	1300	1.39	0.63
AgP_2	8200	14	1100	2.34	1.27
TiP_2	20327	62	1100	0.03	0.03
CuP_2	927	14	1100	1.96	0.93
RuP_2	1413	58	800	0.89	0.33
CoP_2	14285	14	700	1.01	0.36
IrP_2	10155	14	1100	0.85	0.31
BeP_2	27148	15	1300	0.55	0.87
RhP_2	15953	14	800	0.52	0.16
PdP_2	28266	15	600	1.82	0.55
FeP_2	20027	58	500	0.48	0.16
Zn_3P_2	2071	137	900	0.81	0.59
Mg_3P_2	8085	224	1200	2.28	1.46
Mg_3P_2	2514	206	1300	1.82	1.02
Cd_3P_2	2441	137	600	0.50	0.43
MnP_4	569522	2	700	0.31	0.10
MnP_4	487	2	700	0.96	0.20

PbTe	19717	225	1100	2.83	2.60
Bi_2Te_3	568390	166	1000	2.58	2.38

Table S9: Computed charge transfer between the metal and phosphorous atoms. While most compounds have only a small charge transfer between the atoms, the *XY*P subclass has a relative large charge transfer.

Material	mp	Space group	Charge Transfer
BP	1479	216	B: +0.40; P: -0.40
GaP	2490	216	Ga: +0.78; P: -0.78
FeP	1005	62	Fe: +0.31; P: -0.31
ZnNaP	4824	129	Na: +0.81; Zn: +0.51; P: -1.32
SrLiP	10614	187	Sr: +1.33; Li: +0.81; P: -2.14
BaLiP	10615	187	Ba: +1.20; Li: +0.82; P: -2.02
SnNaP	29529	186	Na: +0.81; Sn: +0.32; P: -1.13
NiP_2	22619	205	Ni: +0.11; P_1: -0.04; P_2: -0.07
NiP_2	486	15	Ni: +0.13; P_1: -0.06; P_2: -0.07
ZnP_2	11025	96	Zn: +0.59; P_1: -0.29; P_2: -0.30
ZnP_2	2782	92	Zn: +0.59; P_1: -0.29; P_2: -0.30
AgP_2	8200	14	Ag: +0.19; P_1: -0.03; P_2: -0.17
TiP_2	20327	62	Ti: +1.36; P_1: -0.84; P_2: -0.52
CuP_2	927	14	Cu: +0.27; P_1: -0.04; P_2: -0.23
RuP_2	1413	58	Ru: +0.07; P_1: -0.03; P_2: -0.04
CoP_2	14285	14	Co: +0.09; P_1: -0.05; P_2: -0.05
IrP_2	10155	14	Ir: -0.16; P_1: +0.09; P_2: +0.07
BeP_2	27148	15	Be: +1.51; P_1: -0.76; P_2: -0.76
RhP_2	15953	14	Rh: -0.04; P_1: +0.01; P_2: +0.04
PdP_2	28266	15	Pd: -0.05; P_1: +0.02; P_2: +0.03
FeP_2	20027	58	Fe: +0.20; P_1: -0.08; P_2: -0.12
Zn_3P_2	2071	137	Zn_1: +0.61; Zn_2: +0.62; Zn_3: +0.63; P_1: -0.91; P_2: -0.95
Mg_3P_2	8085	224	Mg_1: +1.53; Mg_2: +1.53; Mg_3: +1.53; P_1: -2.29; P_2: -2.29
Mg_3P_2	2514	206	Mg_1: +1.56; Mg_2: +1.56; Mg_3: +1.56; P_1: -2.34; P_2: -2.34
Cd_3P_2	2441	137	Cd_1: +0.57; Cd_2: +0.57; Cd_3: +0.57; P_1: -0.85; P_2: -0.87

MnP_4	487	2	Mn: +0.47; P_1: -0.06; P_2: -0.07; P_3: -0.14; P_4: -0.20
MnP_4	569522	2	Mn: +0.47; P_1: -0.06; P_2: -0.07; P_3: -0.14; P_4: -0.20

***Table S10*:** Rietveld refined PXRD data for *c*-NiP_2.

Parameter	*c*-NiP_2
Space group	$Pa\bar{3}$ (No. 205)
a / Å	5.469
b / Å	5.469
c / Å	5.469
α / °	90.000
β / °	90.000
γ / °	90.000
Number of molecules per unit cell, *Z*	4
Volume / $Å^3$	164
Calculated density / g cm^{-3}	4.90
R_p	11.21
R_{wp}	16.96
χ^2	1.65

Atom	Site	*x*	*y*	*z*	Occupation
Ni	4*a*	0.000	0.000	0.000	1.000
P	8*c*	0.385	0.385	0.385	2.001

***Table S11*:** Heat capacity data for *c*-NiP_2 using ^{4}He cooling: *27.82±0.01* mg; in order of data collection.

T / K	C_p / J K^{-1} mol^{-1}	T / K	C_p / J K^{-1} mol^{-1}	T / K	C_p / J K^{-1} mol^{-1}
303.64	66.96	53.29	7.99	9.96	0.13
283.41	65.83	48.28	6.32	9.02	0.11
263.26	63.06	43.74	4.96	8.17	0.09
243.06	60.55	39.62	3.87	7.40	0.08
222.89	57.95	35.91	2.99	6.70	0.07
202.69	54.63	32.53	2.31	6.08	0.06
182.48	50.84	29.48	1.78	5.49	0.06
162.27	46.19	26.71	1.38	4.98	0.05
142.05	40.57	24.21	1.05	4.51	0.05
121.79	34.15	21.94	0.82	4.08	0.04
101.57	26.67	19.89	0.64	3.70	0.04
96.53	24.58	18.02	0.49	3.35	0.04
87.45	20.71	16.33	0.39	3.03	0.04
79.24	17.70	14.78	0.31	2.74	0.04
71.75	14.92	13.40	0.25	2.49	0.03
65.06	12.09	12.14	0.20	2.25	0.03
58.84	9.97	11.00	0.16	2.04	0.03

***Table S12*:** Heat capacity data for *c*-NiP_2 using ^{3}He cooling: *21.01±0.01* mg; in order of data collection.

T / K	C_p / J K^{-1} mol^{-1}	T / K	C_p / J K^{-1} mol^{-1}	T / K	C_p / J K^{-1} mol^{-1}
301.88	69.855	3.45	0.032	1.10	0.016
10.05	0.125	3.17	0.031	1.02	0.015
9.26	0.106	2.92	0.029	0.94	0.014
8.52	0.091	2.69	0.028	0.87	0.013
7.85	0.079	2.48	0.027	0.80	0.012
7.22	0.069	2.29	0.026	0.74	0.011
6.65	0.060	2.11	0.025	0.69	0.010
6.13	0.054	1.94	0.024	0.63	0.009
5.65	0.049	1.79	0.023	0.59	0.009
5.20	0.045	1.65	0.022	0.54	0.008
4.79	0.041	1.52	0.020	0.50	0.008

4.41	0.039	1.40	0.019	0.46	0.008
4.07	0.036	1.29	0.018	0.43	0.007
3.74	0.034	1.19	0.017		

***Table S13*:** Experimental electrical resistivity (ρ) for *c*-NiP_2; in order of data collection. Low-temperature (LT) measurements were conducted with a two-probe method in a Quantum Design PPMS while high-temperature (HT) ρ were measured using the van der Pauw technique. It is important to note that the LT data were empirically adjusted to the HT data at T = 312 K, using a contact resistance (10 mΩ; $\rho_{contact}$ = 24 mΩ cm). HT measurements have an uncertainty of 5%.

T / K	ρ (LT) /mΩ cm	T / K	ρ (HT) /mΩ cm	T / K	ρ (HT) /mΩ cm	T / K	ρ (HT) /mΩ cm	T / K	ρ (HT) /mΩ cm
312.27	9.11	295.25	9.05	406.55	8.21	516.15	7.39	626.15	6.37
292.29	9.63	298.45	9.01	411.45	8.17	521.05	7.34	630.95	6.33
272.33	10.21	299.65	8.99	415.95	8.14	525.85	7.31	635.65	6.28
252.40	10.72	304.75	8.93	420.75	8.1	530.45	7.27	640.45	6.24
226.92	11.29	314.05	8.86	425.85	8.06	535.35	7.23	645.45	6.19
202.04	11.74	321.85	8.82	430.35	8.03	540.35	7.18	649.95	6.15
176.81	12.13	326.15	8.8	435.25	7.99	544.85	7.14	654.55	6.11
151.93	12.43	329.75	8.77	439.85	7.96	549.85	7.1	659.45	6.06
126.76	12.67	334.15	8.73	444.75	7.92	554.35	7.06	664.25	6.01
101.57	12.85	339.45	8.7	449.55	7.89	559.15	7.02	669.05	5.96
81.35	13.03	344.65	8.66	454.25	7.86	563.95	6.97	673.75	5.92
51.09	13.19	349.55	8.62	459.15	7.83	568.55	6.93	678.45	5.87
31.10	13.25	354.25	8.59	463.75	7.8	573.65	6.88	683.35	5.82
20.58	13.28	358.85	8.55	468.65	7.76	578.35	6.84	687.95	5.77
18.55	13.31	363.65	8.52	473.65	7.72	583.15	6.79	692.85	5.71
15.60	13.31	368.65	8.48	478.05	7.69	587.85	6.75	697.65	5.66
10.50	13.36	373.05	8.45	482.85	7.65	592.75	6.7	702.35	5.6
8.29	13.39	377.95	8.42	487.65	7.61	597.55	6.66	707.05	5.55
6.28	13.42	382.75	8.38	492.35	7.58	602.25	6.61	712.05	5.49
4.35	13.48	387.45	8.35	497.15	7.54	607.15	6.56	716.75	5.43
2.41	13.59	392.25	8.32	501.85	7.5	611.65	6.51	721.55	5.37
		397.15	8.28	506.75	7.46	616.75	6.47	726.15	5.31
		401.75	8.25	511.45	7.42	621.35	6.42		

***Table S14*:** Experimental Seebeck coefficient (*S*) for *c*-NiP_2; in order of data collection. Low-temperature (LT) measurements were conducted in a Quantum Design PPMS while high-temperature (HT) *S* were measured with an oscillating temperature gradient. LT and HT measurements have an uncertainty of 5%.

T / K	*S* (LT) / μV K^{-1}	*T* / K	*S* (LT) / μV K^{-1}	*T* / K	*S* (LT) / μV K^{-1}	*T* / K	*S* (HT) / μV K^{-1}
391.86	-40.86	176.81	-29.24	10.50	-0.86	324.55	-37.63
371.97	-40.73	151.93	-26.53	8.29	-2.54	369.63	-40.98
352.10	-41.00	126.76	-23.54	4.35	-1.73	415.88	-44.27
332.22	-39.67	101.57	-16.15	2.41	-1.41	462.83	-47.51
312.28	-39.06	81.35	-15.25			511.20	-50.75
292.29	-39.48	51.09	-10.06			559.07	-55.08
272.33	-37.66	31.10	-4.79			606.79	-57.65
252.40	-36.56	20.58	-2.89			654.87	-55.60
226.92	-34.63	18.55	-3.97			701.40	-51.51
202.04	-32.18	15.60	-2.02			748.50	-44.77

***Table S15*:** Experimental thermal conductivity (κ) for *c*-NiP_2; in order of data collection. Low-temperature (LT) measurements were conducted in a Quantum Design PPMS where the thermal conductivity was corrected for blackbody radiation with an emissivity of 1. High-temperature (HT) κ was calculated from the thermal diffusivity (α), the density (*d*), and the computed heat capacity (C_p). While the LT measurement has an uncertainty of 5%, the HT measurement has an uncertainty of 15%.

T / K	κ (LT) / W m^{-1} K^{-1}	*T* / K	κ (LT) / W m^{-1} K^{-1}	*T* / K	α / mm^2 s^{-1}	*d* / g cm^{-3}	C_p / J g^{-1} K^{-1}	κ(HT) / W m^{-1} K^{-1}
312.28	1.16	51.09	0.33	323.45	0.40	4.04	0.57	0.92
292.29	1.12	31.10	0.17	375.15	0.41	4.04	0.59	0.97
272.33	1.08	20.58	0.09	425.45	0.41	4.04	0.61	1.00
252.40	1.05	18.56	0.08	475.15	0.42	4.04	0.62	1.04
226.92	0.99	15.62	0.06	524.95	0.43	4.04	0.62	1.07
202.04	0.94	10.51	0.03	574.55	0.44	4.04	0.63	1.11
176.81	0.88	8.30	0.02	624.35	0.45	4.04	0.63	1.16
151.93	0.86	6.30	0.01	674.25	0.47	4.04	0.63	1.20
126.76	0.75	4.36	0.01	724.15	0.48	4.04	0.64	1.24
101.57	0.62	2.42	0.00					

81.35	0.52							

[1] Y. Kumashiro, M. Hirabayashi, T. Koshiro, Y. Okada, *J. Less-Common Metals* **1988**, *143*, 159–165.
[2] D. G. Cahill, S. K. Watson, R. O. Pohl, *Phys. Rev. B* **1992**, *46*, 6133-6140.
[3] D. G. Cahill, R. O. Pohl, *Ann. Rev. Phys. Chem.* **1988**, *39*, 93-121.
[4] M. de Jong, W. Chen, T. Angsten, A. Jain, R. Notestine, A. Gamst, M. Sluiter, C. K. Ande, S. Van Der Zwaag, J. J. Plata, C. Toher, S. Curtarolo, G. Ceder, K. A. Persson, M. Asta, *Sci. Data* **2015**, *2*, 150009.
[5] W. Chen, J.-H. Pöhls, G. Hautier, D. Broberg, S. Bajaj, U. Aydemir, Z. M. Gibbs, H. Zhu, M. Asta, G. J. Snyder, B. Meredig, M. A. White, K. Persson, A. Jain, *J. Mater. Chem. C* **2016**, *4*, 4414-4426.
[6] J.-H. Pöhls, M. B. Johnson, M. A. White, *Phys. Chem. Chem. Phys.* **2016**, *18*, 1185-1190.
[7] A. Einstein, *Ann. Phys.* **1911**, *35*, 679-694.
[8] F. Gillot, S. Boyanov, L. Dupont, M.-L. Doublet, M. Morcrette, L. Monconduit, J.-M. Tarascon, *Chem. Mater.* **2005**, *17*, 6327-6337.
[9] P. C. Donohue, T.-A. Bither, H. S. Young, *Inorg. Chem.* **1968**, *7*, 998-1001.
[10] G. K. Williamson, W. H. Hall, *Acta Metall.* **1953**, *1*, 22-31.
[11] S. A. Miller, P. Gorai, B. R. Ortiz, A. Goyal, D. Gao, S. A. Barnett, T. O. Mason, G. J. Snyder, Q. Lv, V. Stevanović, E. S. Toberer, *Chem. Mater.*. **2017**, *accepted*.